SAND2015-6277J

Journal of Colloid and Interface Science

Surface-Assisted Formation of Methane Hydrates on Ice and Na-Montmorillonite Clay

Margaret E. Gordon[a], Stephanie L. Teich-McGoldrick[b], Randall T. Cygan[b], Stephen P. Meserole[c], Mark A. Rodriguez[d]
[a.] Department of Materials, Devices, and Energy Technologies
[b.] Geochemistry Department
[c.] Electronic, Optical, & Nano Materials Department
[d.] Materials Characterization Department
Sandia National Laboratories, Albuquerque, NM, 87185 USA

Abstract:

Methane hydrates are extremely important naturally-occurring crystalline materials that impact climate change, energy resources, geological hazards, and other major environmental issues. Whereas significant experimental effort has been completed to understanding the bulk thermodynamics of methane hydrate assemblies, little is understood on heterogeneous nucleation and growth of methane hydrates in clay-rich environments. Controlled synthesis experiments were completed at 265-285 K and 6.89 MPa to examine the impact of montmorillonite surfaces in clay-ice mixtures to nucleate and form methane hydrate. The results suggest that the hydrophilic and methane adsorbing properties of Na-montmorillonite reduce the nucleation period of methane hydrate formation in pure ice systems.

Keywords: methane hydrate, montmorillonite clay, substrate, clathrate hydrate, nucleation period, ice

Introduction: Methane hydrates are a class of clathrate compounds that form under high pressure and low temperature conditions (generally greater than 3.5 MPa and less than 280 K) with ice-like cages surrounding one or more methane molecules.[1] Several methane hydrate structures exist, and the two most common types, isometric structure I and structure II, are formed of both small and large H_2O cages. Structure I is built of two small cages consisting of 12 pentagonal faces (5^{12} cages), and six large cages that have 12 pentagonal faces and 2 hexagonal faces ($5^{12}6^2$ cages). The larger unit cell of structure II consists of sixteen 5^{12} and eight $5^{12}6^4$ cages.[1]

Methane hydrates form naturally in ocean floor sediments associated with gas vents.[1] Deep water oil pipelines present ideal thermodynamic (sub-zero temperatures and high pressure) and chemical (methane in contact with sea water) conditions for the formation of methane hydrates that can lead to pipeline blockages.[1] Large untapped hydrate reserves also exist in the Arctic seafloor and a recent U.S

Geological survey estimates that 590 trillion cubic feet (or over 14000 km^3) of methane hydrate is present in the permafrost on the North Slope of Alaska.[2]–[4] At ambient conditions, methane hydrates decompose to produce methane and water, making them of interest as an energy resource or as potential energy carriers. At the same time, if destabilized through warming or other disruptive processes, natural formations of methane hydrate could release large amounts of methane, a recognized greenhouse gas considerably more impactful to the climate than CO_2.[5] The ability to utilize and control hydrate resources is currently hindered by a lack of fundamental understanding of the impact of geological setting and conditions on the stability and formation of methane hydrates, which are typically found in clay-rich sediments.

Prior work on understanding the formation of hydrates on ice and water [6]–[10][11]–[15][16][17] has revealed several key parameters and stages in methane hydrate growth. The size of the gas-ice contact area correlates directly with the formation of methane hydrate as shown in early work by Barrer.[18] A study by Wang on the kinetics of methane hydrate formation on deuterated ice calculated the activation energy to be 61.5 kJ/mol.[19] Several models have been proposed for methane hydrate formation, including a shrinking ice core model,[20], [21] a diffusion model[9], and a quasi-liquid redistribution model.[22] Laboratory investigations have elucidated two recognized stages in hydrate formation on ice.[6], [7], [23] First, a nucleation event occurs at a high energy surface site or interface such as a crack, step edge, or contact point between ice particles. Hydrate forms, spreading across the ice-grain surface creating a “shell” of hydrate around the ice particles. The second stage of hydrate formation occurs via two potential pathways—hydrate on hydrate growth via diffusion of water through the hydrate shell formed in stage 1, or “sub-shell” hydrate growth from gas diffusion through the hydrate shell to the ice surface. While there is evidence supporting hydrate formation through these stages, additional simulation investigations separating the nucleation events, spreading events, and bulk growth events are required to fully understand their synergy and controlling parameters.[24] Current ongoing work in our laboratories is examining these systems at the molecular scale with simulation to understand growth kinetics in both homogenous and heterogeneous media.

Formation of natural methane hydrates occurs in numerous submarine basins, each exhibiting unique sediment characteristics. Several studies have investigated the stability, kinetics, and spatial distribution of hydrates[25]–[29] on diverse ocean sediments. Many of these studies, however, focus on methane-saturated water in a stirred reactor and reactions can require several days.[11], [30], [31] Reactions are limited by mass and heat transfer. In more specialized experimental reactors, Kang and Seo (2008) investigated porous silica and determined that the porous silica surface inhibited the thermodynamics of growth, raising the temperature at which methane hydrate growth commenced by 1 – 1.5 K.[32] Further studies of hydrate nucleation on porous silica have shown that the smaller the pore size, the greater the growth inhibition effect.[33], [34] The influence of clay mineral surfaces[35] was investigated and found that bentonite particles assist in the formation of methane hydrates, requiring a lower driving force of 0.66 MPa at 4.5 °C (277.65 K) instead of >4 MPa in a stirred liquid reactor. Seo et al (2009) investigated methane hydrate formation in the interlayer spaces of Cheto montmorillonite, and found that its higher charge interlayer cation (Ca^{2+} counter cations vs. Na^{+} in other montmorillonite samples) negatively affected the promotion of hydrate growth through structuring of the hydrating waters.[32]

In this paper, the investigation of Na-montmorillonite clay surface-mediated formation of methane hydrates from a cold, dry, static system of ice and clay is reported. Substrates consisted of pure ice and three relatively low amounts of Na-montmorillonite (5%, 10%, and 15% by weight) mixed with ice. A comparison of the required time for each system to initiate hydrate formation (the nucleation period) is presented and discussed.

Materials and Methods:

Natural Wyoming Na-Montmorillonite (MMT) (SWy-2, Source Clays Repository, administered by the Clay Minerals Society) and UHP grade methane from Trigas were used as received. The surface area of MMT was measured via BET (Micromeritics ASAP 2010) to be 17.55 +/-0.25 m^2/g.

The synthesis procedure is similar to that reported in Stern et al.[8] Gas-free ice (20.0g) precooled to -26 °C (247.15 K) was pulverized, weighed, and placed in a pre-cooled Teflon cup. For samples containing clay, the ice was pulverized, and then mixed with pre-cooled clay in the appropriate weight percentage (5, 10, and 15%). The added surface area of the clay varied from 17.55 m^2, to 35.10 m^2, and to 52.65 m^2. These values correspond to an added surface area of 0.84 m^2/g, 1.60 m^2/g, and 2.29 m^2/g of the clay-ice mixtures, respectively. The cup was then capped, and placed in a pre-cooled Parr reactor (Model 4651-High Pressure Vessel, 250 mL volume) located in a programmable chest freezer (Freezer Concepts CH40-13 Chest Freezer). The initial system temperature (freezer and reactor) was -26 °C (247.15 K). After evacuation and purging with pre-cooled N_2, and then purging with precooled CH_4, the reactor was pressurized to 6.89 MPa with pre-cooled CH_4 and allowed to equilibrate. The temperature and internal pressure of the reactor were recorded throughout, as was the temperature of freezer. After approximately 30 minutes, the temperature and pressure stabilized. Undercooling of the reactor to 247 K well below the reaction temperature as found in Stern et al., ensures that the temperature increase of the methane gas during the adiabatic expansion from the precooling chamber into the reaction vessel does not approach the melting point of ice.[36]

The freezer was then programmed to warm at 3.5 K/hr. As the temperature increased and exceeded the melting point of water, the reactor achieved an isothermal state as the ice melted. In the presence of free water and ice under 6.89 MPa of CH_4, the methane pressure dropped as methane hydrate formed. The time from equilibrium to the inflection of the pressure curve was measured. (Specifically, the time from a defined starting temperature of 268.15 K to the divergence of the pressure data curve from the temperature data curve was measured.) A control experiment with ice and nitrogen (6.89 MPa) was performed; that data is available in the supporting information.

Data was normalized using the following protocol. A starting temperature for each experiment was set to 268.15 K. The pressure data were then corrected to normalize the pressure for the temperature profile for each experiment and adjust each starting pressure to 6.89 MPa:

$$P_{corrected} = P_{measured} - [(P_{start} - 6.89)T_{measured}]/T_{start} \quad (1)$$

Samples for Raman spectroscopy and powder X-ray diffraction were obtained using the following procedure. Pulverized gas free ice was loaded into a pre-cooled Teflon cup. The cup was capped, and the

Parr reactor was sealed. The experiment then proceeded as described above. After 250 minutes, including 100 minutes in the hydrate forming region, the pressurized reactor was cooled to 248.15 K. The reactor was vented, and the capped Teflon sample cup was removed and placed in a container with liquid nitrogen (77.2 K).

To obtain Raman data, the cooled sample was removed from the liquid nitrogen, placed into a quartz cuvette that had been cooled in liquid nitrogen before being placed in the Macro chamber of a Horiba T64000 Raman Spectrometer fitted with 600 grooves/mm gratings. A green laser (514.532nm laser at 10mW before entering the instrument) was used for excitation. The instrument was calibrated by placing a sample of powdered LDPE (in a quartz cuvette holder) into the Macro chamber and acquiring a spectrum. The methane-hydrate spectrum shown was captured using 10 accumulations of 10 seconds. The time from Parr reactor depressurization to complete the data capture was less than 45 minutes. See Figure 1.

Powder X-ray diffraction data using a Bruker Venture Single Crystal diffractometer was obtained in the following manner. The synthesized methane hydrate powder was scooped out of the LN_2 cooled beaker and onto either a glass fiber or on Mylar-tipped loops which was subsequently mounted quickly onto the instrument. Both materials add minimal signal to the pattern in terms of sharp reflections in the 2θ diffraction pattern. The fast transfer of the sample was necessary to prevent warming and decomposition of the methane hydrate material. Once mounted, the sample was held under a cold-stream of gaseous N_2 at 100 K. A microfocused X-ray source (Cu radiation) was employed for XRD analysis with a spot size of ~100 micron for the beam at the sample location. Incident beam mirror optics conditioned the x-ray beam to a monochromatic wavelength. The powder was spun on the phi axis to improve randomization of the powder during collection. A 60-second frame time was employed and data were collected using a CMOS Photon 100 detector. Area detector data were reduced to a 1D pattern via APEX II software and the subsequent patterns were analyzed via JADE (V9.6) software for phase identification. See Figure 1.

Results:

Experimental hydrate nucleation runs, following the above procedure, result in the reproducible formation of methane hydrate with remnant ice in the pressure vessel. The starting conditions of 6.89 MPa and 268K (undercool ΔT = 5K) were chosen to be within the ice and methane hydrate stability region. Owing to the absence of liquid water, however, the formation of methane hydrate under these conditions is kinetically unfavored.[37] These starting conditions, therefore, allow the system to equilibrate for <60 minutes without the risk of hydrate formation.

All experiments proceed following identical steps as presented by Stern[8] and Staykova [7]. At initial conditions, the reaction vessel is at 6.89 MPa pressure, and ice and methane exist in equilibrium. These phases persist as the reaction vessel temperature increases until reaching the melting point of ice. (See reaction diagram Figure 2.) Near 273 K, liquid water appears[7], [8] in the system on the surface of the ice grains and the reaction vessel enters an isothermal period. Prior work using SEM [6], [7] shows that in a pure system the first methane hydrate crystals form at the interstices of the ice grains once liquid

water is present. The exothermic nature [6], [12] of the hydrate formation reaction further drives the phase change of H_2O and therefore hydrate formation reaction as well. Growth continues across the surface of the ice grain as the methane hydrate forms from the water present. At the temperature ramp rate used in these experiments, the reaction vessel reaches the methane hydrate dissociation point (~282 K) before the water is completely consumed in the reaction. As the focus of this work is the initial formation of hydrate, complete conversion of the solid water to methane hydrate was unnecessary. Raman spectroscopic data and powder XRD were used to confirm both the presence of sI hydrate and ice after 240 minutes. The Raman peaks present at 2907 and 2914 cm^{-1} are characteristic of the methane stretching modes of CH_4 molecules enclosed in hydrate cages. [38] See Figure 1. Further confirmation is provided by the collected powder XRD pattern which clearly shows overlapping ice and methane hydrate peaks. See Figure 1. A relative intensity ratio analysis of the XRD data suggests that the sample is approximately 42 wt% methane hydrate with the balance being composed of ice. Visual inspection of the reaction products in the vessel indicate the characteristic hydrate texture and popping sound associated with hydrate decomposition and methane release.

Inclusion of montmorillonite clay surfaces in the reaction vessel has several noticeable effects on the reaction sequence. First, the time required to reach the methane pressure drop from time zero decreases, suggesting that the methane hydrate nucleation period is reduced in the presence of dispersed clay particles. To determine the nucleation period, two tangential trend lines for the constant slope areas before and after the deflection in the pressure-time curve were extended until they crossed. This point we term “the deflection point” which represents the end point of the nucleation period. The elapsed time of the nucleation period and the temperature of the identified pressure at the deflection point were then graphed for each sample. See Figure 3. Under the investigated conditions, the reduction in the methane hydrate nucleation period is independent of the wt% of the clay in the mixture over the range investigated. At higher loadings of MMT, however, several pressure deflections occur independent of temperature in the region of methane hydrate formation, and will require further investigation to fully evaluate.

Discussion:

SWy-2 Na-Montmorillonite clay (MMT) is a 2:1 phyllosilicate characterized by layers comprised of two sheets of tetrahedrally-coordinated Si sandwiched about a central sheet of octahedrally-coordinated Al(Mg). Multiple layers are ordered into nanoparticles that have relatively poor crystallinity and limited long range stacking order. SEM analysis of MMT revealed aggregates of clay platelets on the order of 30 nm in size, which was further confirmed by powder XRD and the use of the Scherrer equation to ascertain the average particle size.[39] SWy-2 Na-MMT is known for limited substitution of Mg^{2+} for Al^{3+} in the octahedral sheet. The layer charge requires counter cations in the interlayer spaces. Elemental analysis of the SWy-2 Na-MMT, presented in Table 1, shows that a majority of these charge balancing ions are Na^{+}.[40]

Table 1: Composition of SWy-2 Na-MMT [37]

Elemental Analysis	**Mass fraction**
Si	59.600

Al_2O_3	22.800
Fe_2O_3	47.725
MgO	3.400
CaO	1.140
Na_2O	2.451
K_2O	0.549
TiO_2	0.160
P_2O_5	0
MnO	0.036
Cr_2O_3	0.017
S	0.188
Structural formula	
$(Ca_{0.12}Na_{0.32}K_{0.05})[Al_{3.01}Fe(III)_{0.41}Mn_{0.01}Mg_{0.54}Ti_{0.02}][Si_{7.98}Al_{0.02}]O_{20}(OH)_4 \cdot nH_2O$	

Hydrate growth from ice has been postulated to occur first at interstices;[6], [7] in the presented synthesis of methane hydrate involving the clay-ice mixtures, there are three possible types of interstices: ice-ice, ice-clay, and clay-clay. In this series of experiments, the relative amount of MMT is kept small and is dry-mixed with the pulverized ice. Clay particles are most likely dispersed during mixing, surrounded by ice rather than other clay surfaces. During the warming phase, the primary exposed surface is ice or ice with a layer of water on it with a small fraction of clay surface area.

Adsorption of methane on clay external surfaces and into clay interlayers in the early phase of the reaction must be considered. Adsorption capacity studies examined at similar elevated pressures (6.89 MPa) show relatively high methane adsorption capacities around 4.3 cm^3/g at 60 °C.[41] The lower temperature in this work will increase the affinity of clay surfaces for methane at these high pressures. Simulations in earlier work have shown the methane-MMT adsorption to be controlled by weak van der Waals-type interactions.[42] In the early reaction phase, methane molecules will be adsorbed to all exposed clay surfaces.

More significantly, the surfaces and interlayers of the clay will attract water. MMT is known to swell taking in 6 cm^3/g of water into the interlayer spaces. Hydration and wetting of MMT clay surfaces depends primarily on the charge balancing counter ions. Unlike Ca^{2+} in other MMT samples, the hydration layer surrounding the smaller low-charge sodium ions in SWy-2 Na-MMT is loosely held. This is of primary importance in the methane hydrate reaction as these less-strongly bound water molecules are available to react with methane to form the hydrate. Simulations have previously revealed that the water-clay interaction is stronger than the methane-clay interaction.[42]

The effects of methane adsorption and wettability combine to lower the nucleation time for methane hydrate formation in the presence of SWy-2 Na MMT under the given conditions. See Figure 3. In the initial warming phase of the reactions, methane is adsorbed onto the exposed external surfaces of MMT and on exposed ice. As the melting point of ice is reached (273 K after approximately 90 minutes), mobile water is now available to associate with the clay surfaces and will displace the methane adsorbed on the clay surfaces. Under the reaction conditions, the adsorbed methane on the ice and clay

surfaces and melted ice react quickly to form methane hydrate, indicated by the decrease in methane pressure that occurs less than 31 minutes after the melting point of ice is achieved, at 117 to 119.5 minutes (the longest nucleation) period of any of the clay loaded systems). Without the presence of clay surfaces, methane diffuses into the liquid water phase on the ice particle surfaces to eventually react and form methane hydrate about 50 minutes after the melting point of ice between 141 and 144 minutes. This is an increase of more than 20 minutes in nucleation time to form the methane hydrate compared to the MMT systems under equivalent reaction conditions. Further *in situ* surface studies are underway to better elucidate the fundamentals of the fundamental reaction steps.

Conclusions:

Dispersed montmorillonite particles on ice were shown to decrease the nucleation time by approximately 20 minutes for methane hydrate growth relative to hydrate formation on melting ice surfaces for our experimental conditions. Experiments using variable clay loading (5, 10, and 15 wt %) with ice show nucleation times of 119 minutes (about 30 minutes after the melting point of ice) for methane hydrate formation. The identical system without clay has a nucleation period of more than 140 minutes (about 50 minutes after the melting point of ice). No further decrease was evident for higher loadings of the clay in these clay-ice mixtures. The presence of the Na-MMT clay surface that adsorbs methane, and which is hydrophilic, serves to facilitate hydrate formation. Further studies to elucidate hydrate growth mechanisms on the clay surfaces using *in situ* spectroscopic monitoring are in progress, along with large-scale molecular dynamics simulations.

Acknowledgements:

We would like to thank Jeffery Greathouse, Konrad Thürmer, David Tallant, Andrea Ambrosini, and Anthony Martino for their helpful technical suggestions, and for reviews of the original manuscript. This work is supported by the Laboratory Directed Research and Development program at Sandia National Laboratories. Sandia National Laboratories is a multi-program laboratory managed and operated by Sandia Corporation, a wholly owned subsidiary of Lockheed Martin Corporation, for the U.S. Department of Energy's National Nuclear Security Administration under Contract DE-AC04–94AL85000.

[1] E. D. Sloan and C. Koh, *Clathrate Hydrates of Natural Gases, Third Edition*, 3rd ed. CRC Press.
[2] K. A. Kvenvolden and M. A. McMenamin, "Hydrates of Natural Gas: A Review of Their Geologic Occurrence," Geological Survey Circular 825, 1980.
[3] T. S. Collett, "Natural Gas Hydrates of the Prudhoe Bay and Kuparuk River Area, North Slope, Alaska," *AAPG Bull.*, vol. 77, no. 5, pp. 793–812, 1993.
[4] T. S. Collett, M. W. Lee, W. F. Agena, J. J. Miller, K. A. Lewis, M. V. Zyrianova, R. Boswell, and T. L. Inks, "Permafrost-associated natural gas hydrate occurrences on the Alaska North Slope," *Mar. Pet. Geol.*, vol. 28, no. 2, pp. 279–294, Feb. 2011.
[5] K. A. (Geological S. Kvenvolden, "Methane Hydrates and Global Climate," *Glob. Biogeochem. Cycles USA*, vol. 2:3, Sep. 1989.
[6] W. F. Kuhs, D. K. Staykova, and A. N. Salamatin, "Formation of Methane Hydrate from Polydisperse Ice Powders," *J. Phys. Chem. B*, vol. 110, no. 26, pp. 13283–13295, Jul. 2006.
[7] D. K. Staykova, W. F. Kuhs, A. N. Salamatin, and T. Hansen, "Formation of Porous Gas Hydrates from Ice Powders: Diffraction Experiments and Multistage Model," *J. Phys. Chem. B*, vol. 107, no. 37, pp. 10299–10311, Sep. 2003.
[8] L. A. Stern, S. H. Kirby, W. B. Durham, S. Circone, and W. F. Waite, "Laboratory synthesis of pure methane hydrate suitable for measurement of physical properties and decomposition behavior," in *Natural Gas Hydrate*, Springer, 2003, pp. 323–348.
[9] S. Takeya, T. Ebinuma, T. Uchida, J. Nagao, and H. Narita, "Self-preservation effect and dissociation rates of CH4 hydrate," *J. Cryst. Growth*, vol. 237–239, Part 1, pp. 379–382, Apr. 2002.
[10] Y. Halpern, V. Thieu, R. W. Henning, X. P. Wang, and A. J. Schultz, "Time-resolved in situ neutron diffraction studies of gas hydrate: Transformation of structure II (sII) to structure I (sI)," *J. Am. Chem. Soc.*, vol. 123, no. 51, pp. 12826–12831, Dec. 2001.
[11] P. S. R. Prasad, V. D. Chari, D. V. S. G. K. Sharma, and S. R. Murthy, "Effect of silica particles on the stability of methane hydrates," *Fluid Phase Equilibria*, vol. 318, pp. 110–114, Mar. 2012.
[12] C. V. V. Eswari, B. Raju, V. D. Chari, P. S. R. Prasad, and K. Sain, "Laboratory study of methane hydrate formation kinetics and structural stability in sediments," *Mar. Pet. Geol.*, vol. 58, pp. 199–205, Dec. 2014.
[13] V. D. Chari, D. V. S. G. K. Sharma, P. S. R. Prasad, and S. R. Murthy, "Methane hydrates formation and dissociation in nano silica suspension," *J. Nat. Gas Sci. Eng.*, vol. 11, pp. 7–11, Mar. 2013.
[14] V. D. Chari, B. Raju, P. S. R. Prasad, and D. N. Rao, "Methane Hydrates in Spherical Silica Matrix: Optimization of Capillary Water," *Energy Fuels*, vol. 27, no. 7, pp. 3679–3684, Jul. 2013.
[15] V. D. Chari, P. S. R. Prasad, and S. R. Murthy, "Structural stability of methane hydrates in porous medium: Raman spectroscopic study," *Spectrochim. Acta. A. Mol. Biomol. Spectrosc.*, vol. 120, pp. 636–641, Feb. 2014.
[16] K. Lee, S.-H. Lee, and W. Lee, "Stochastic nature of carbon dioxide hydrate induction times in Na-montmorillonite and marine sediment suspensions," *Int. J. Greenh. Gas Control*, vol. 14, pp. 15–24, May 2013.
[17] T. Koga, J. Wong, M. K. Endoh, D. Mahajan, C. Gutt, and S. K. Satija, "Hydrate Formation at the Methane/Water Interface on the Molecular Scale," *Langmuir*, vol. 26, no. 7, pp. 4627–4630, Apr. 2010.
[18] R. M. Barrer and A. V. J. Edge, "Gas Hydrates Containing Argon, Krypton and Xenon: Kinetics and Energetics of Formation and Equilibria," *Proc. R. Soc. Lond. Math. Phys. Eng. Sci.*, vol. 300, no. 1460, pp. 1–24, Aug. 1967.
[19] X. Wang, A. J. Schultz, and Y. Halpern, "Kinetics of Methane Hydrate Formation from Polycrystalline Deuterated Ice," *J. Phys. Chem. A*, vol. 106, no. 32, pp. 7304–7309, Aug. 2002.
[20] G. Von Froment and K. Bischoff, *Chemical Reactor Analysis and Design.*, 2nd ed. New York: Wiley & Sons, 1990.

[21] O. Levenspiel, “Chemical Reaction Engineering,” *Ind. Eng. Chem. Res.*, vol. 38, no. 11, pp. 4140–4143, Nov. 1999.
[22] Y. Mizuno and N. Hanafusa, “Studies of Surface-Properties of Ice Using Nuclear-Magnetic-Resonance,” *J. Phys.*, vol. 48, no. C–1, pp. 511–517, Mar. 1987.
[23] G. Genov, W. F. Kuhs, D. K. Staykova, E. Goreshnik, and A. N. Salamatin, “Experimental studies on the formation of porous gas hydrates,” *Am. Mineral.*, vol. 89, no. 8–9, pp. 1228–1239, Sep. 2004.
[24] B. C. Barnes and A. K. Sum, “Advances in molecular simulations of clathrate hydrates,” *Curr. Opin. Chem. Eng.*, vol. 2, no. 2, pp. 184–190, May 2013.
[25] M. B. Clennell, M. Hovland, J. S. Booth, P. Henry, and W. J. Winters, “Formation of natural gas hydrates in marine sediments 1. Conceptual model of gas hydrate growth conditioned by host sediment properties,” *J. Geophys. Res.*, vol. 104, no. B10, pp. 22985–23003, Oct. 1999.
[26] P. Henry, M. Thomas, and M. B. Clennell, “Formation of natural gas hydrates in marine sediments 2. Thermodynamic calculations of stability conditions in porous sediments,” *J. Geophys. Res.*, vol. 104, no. B10, pp. 23005–23022, Oct. 1999.
[27] H. Lu, T. Kawasaki, T. Ukita, I. Moudrakovski, T. Fujii, S. Noguchi, T. Shimada, M. Nakamizu, J. Ripmeester, and C. Ratcliffe, “Particle size effect on the saturation of methane hydrate in sediments – Constrained from experimental results,” *Mar. Pet. Geol.*, vol. 28, no. 10, pp. 1801–1805, Nov. 2011.
[28] M. W. Lee and T. S. Collett, “Unique problems associated with seismic analysis of partially gas-saturated unconsolidated sediments,” *Mar. Pet. Geol.*, vol. 26, no. 6, pp. 775–781, Jun. 2009.
[29] T. Collett, J.-J. Bahk, R. Baker, R. Boswell, D. Divins, M. Frye, D. Goldberg, J. Husebo, C. Koh, M. Malone, M. Morell, G. Myers, C. Shipp, and M. Torres, “Methane Hydrates in Nature-Current Knowledge and Challenges,” *J. Chem. Eng. Data*, vol. 60, no. 2, pp. 319–329, Feb. 2015.
[30] W. Hao, J. Wang, S. Fan, and W. Hao, “Study on methane hydration process in a semi-continuous stirred tank reactor,” *Energy Convers. Manag.*, vol. 48, no. 3, pp. 954–960, Mar. 2007.
[31] H. K. Abay, T. M. Svartaas, and W. Ke, “Effect of Gas Composition on sII Hydrate Growth Kinetics,” *Energy Fuels*, vol. 25, no. 4, pp. 1335–1341, Apr. 2011.
[32] Y. Seo, J. Seol, S.-H. Yeon, D.-Y. Koh, M. Cha, S.-P. Kang, Y.-T. Seo, J. Bahk, J. Lee, and H. Lee, “Structural, Mineralogical, and Rheological Properties of Methane Hydrates in Smectite Clays,” *J. Chem. Eng. Data*, vol. 54, no. 4, pp. 1284–1291, Apr. 2009.
[33] K. K. Ostergaard, R. Anderson, M. Llamedo, and B. Tohidi, “Hydrate phase equilibria in porous media: effect of pore size and salinity,” *Terra Nova*, vol. 14, no. 5, pp. 307–312, Oct. 2002.
[34] E. Y. Aladko, Y. A. Dyadin, V. B. Fenelonov, E. G. Larionov, M. S. Mel’gunov, A. Y. Manakov, A. N. Nesterov, and F. V. Zhurko, “Dissociation Conditions of Methane Hydrate in Mesoporous Silica Gels in Wide Ranges of Pressure and Water Content,” *J. Phys. Chem. B*, vol. 108, no. 42, pp. 16540–16547, Oct. 2004.
[35] D. Riestenberg, O. West, S. Lee, S. McCallum, and T. J. Phelps, “Sediment surface effects on methane hydrate formation and dissociation,” *Mar. Geol.*, vol. 198, no. 1–2, pp. 181–190, Jun. 2003.
[36] P.-C. Chen, W.-L. Huang, and L. A. Stern, “Methane hydrate synthesis from ice: Influence of pressurization and ethanol on optimizing formation rates and hydrate yield,” *Energy Fuels*, vol. 24, no. 4, p. 14, 2010.
[37] L. A. Stern, S. H. Kirby, W. B. Durham, S. Circone, and W. F. Waite, “Laboratory synthesis of pure methane hydrate suitable for measurement of physical properties and decomposition behavior.,” in *Natural Gas Hydrate In Oceanic and Permafrost Environments*, vol. 5, Dordrecht: Springer Netherlands, 2000, pp. 323–348.
[38] G. V. P. K. K R Ramya, “Raman spectra of vibrational and librational modes in methane clathrate hydrates using density functional theory.,” *J. Chem. Phys.*, vol. 136, no. 17, p. 174305, 2012.

[39] P. Scherrer, “Estimation of the size and structure of colloidal particles by Rontgen rays,” *Chem. Zentralblatt*, no. i, pp. 322–323, 1919 1918.
[40] H. V. Olphen and J. J. Fripiat, *Data Handbook for Clay Materials and Other Non-metallic Minerals*, 1st edition. Oxford ; New York: Pergamon Press, 1979.
[41] D. Liu, P. Yuan, H. Liu, T. Li, D. Tan, W. Yuan, and H. He, “High-pressure adsorption of methane on montmorillonite, kaolinite and illite,” *Appl. Clay Sci.*, vol. 85, pp. 25–30, Nov. 2013.
[42] R. T. Cygan, S. Guggenheim, and A. F. Koster van Groos, “Molecular Models for the Intercalation of Methane Hydrate Complexes in Montmorillonite Clay,” *J. Phys. Chem. B*, vol. 108, no. 39, pp. 15141–15149, Sep. 2004.

Figures:

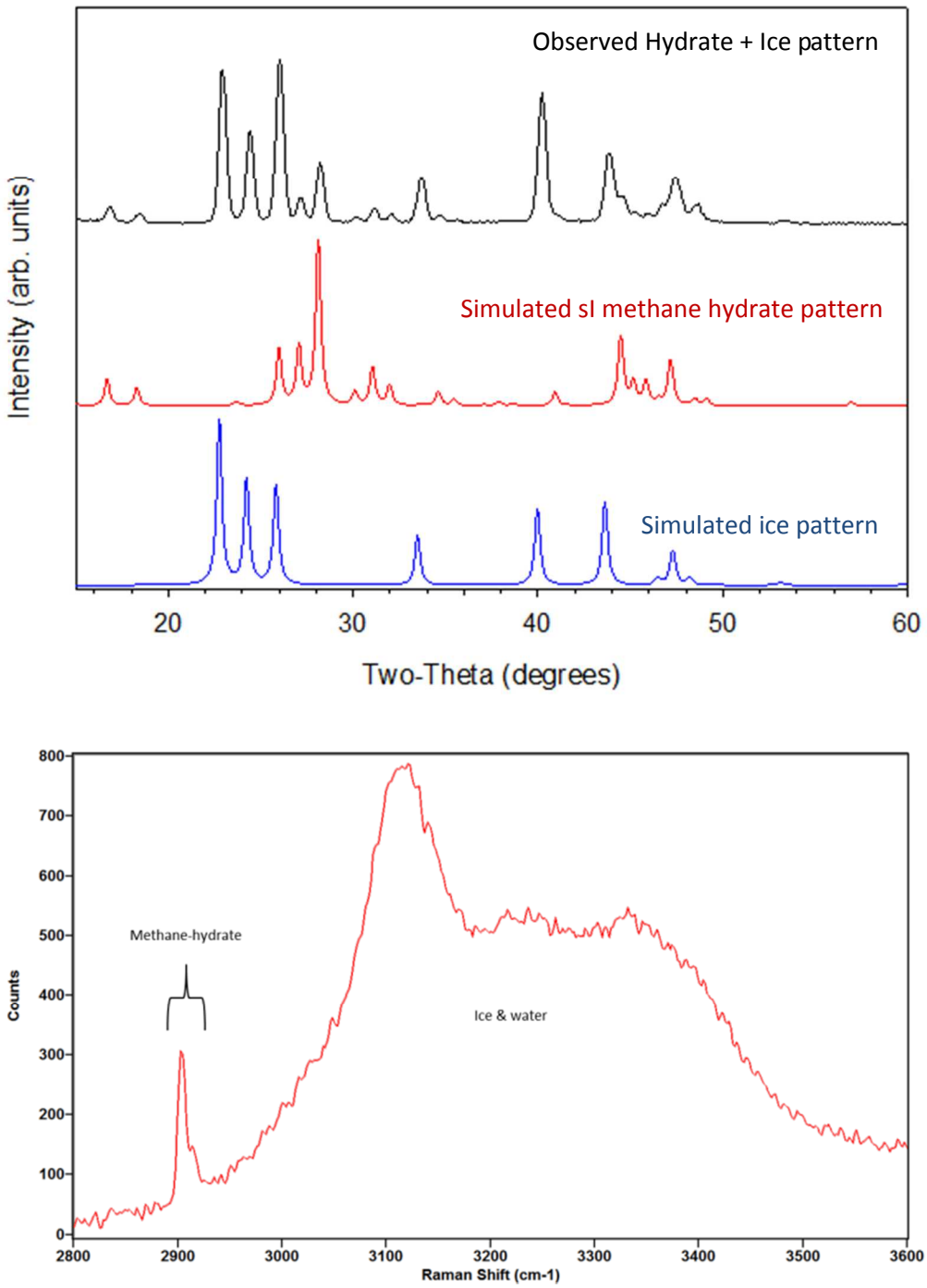

Figure 1. Top: Powder X-ray diffraction pattern of methane hydrate grown on ice (black) and calculated powder patterns of sI methane hydrate (red) and ice (blue). Bottom: Raman spectra of methane hydrate on ice sample at 2904 and 2914 cm^{-1}. The large broad bands are from ice and liquid water.

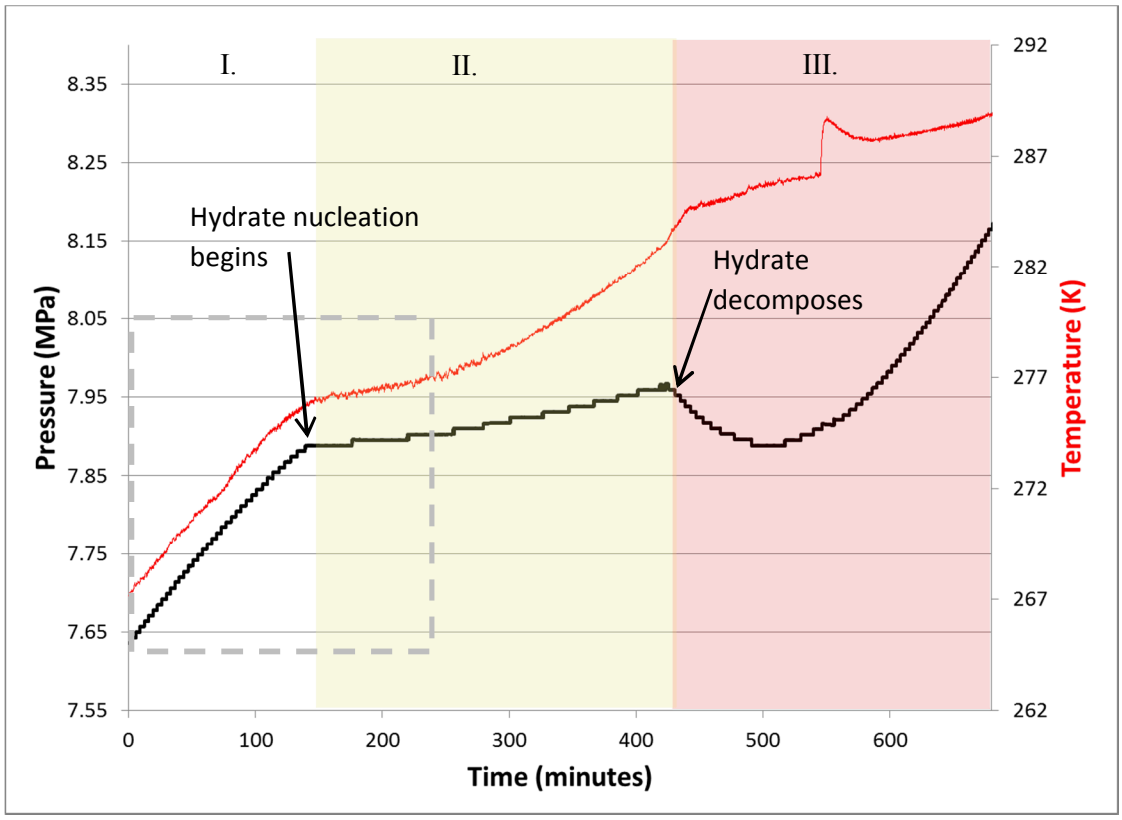

Figure 2 : Pressure versus time data of methane + ice reaction with phase spaces delineated by shaded areas. Black line denotes the pressure data, the red line denotes the temperature data. The non-shaded area (I) represents the phase space where ice and methane are present. The yellow shaded area (II) represents the phase space where ice, water, methane, and methane hydrate coexist. The red shaded area (III) represents the area in which methane hydrate is no longer stable, and decomposes to water and methane. The gray-dashed outline box at left is expanded in Figure 3. A full phase diagram for the methane–ice–methane hydrate system is published under Stern et. al. [37]

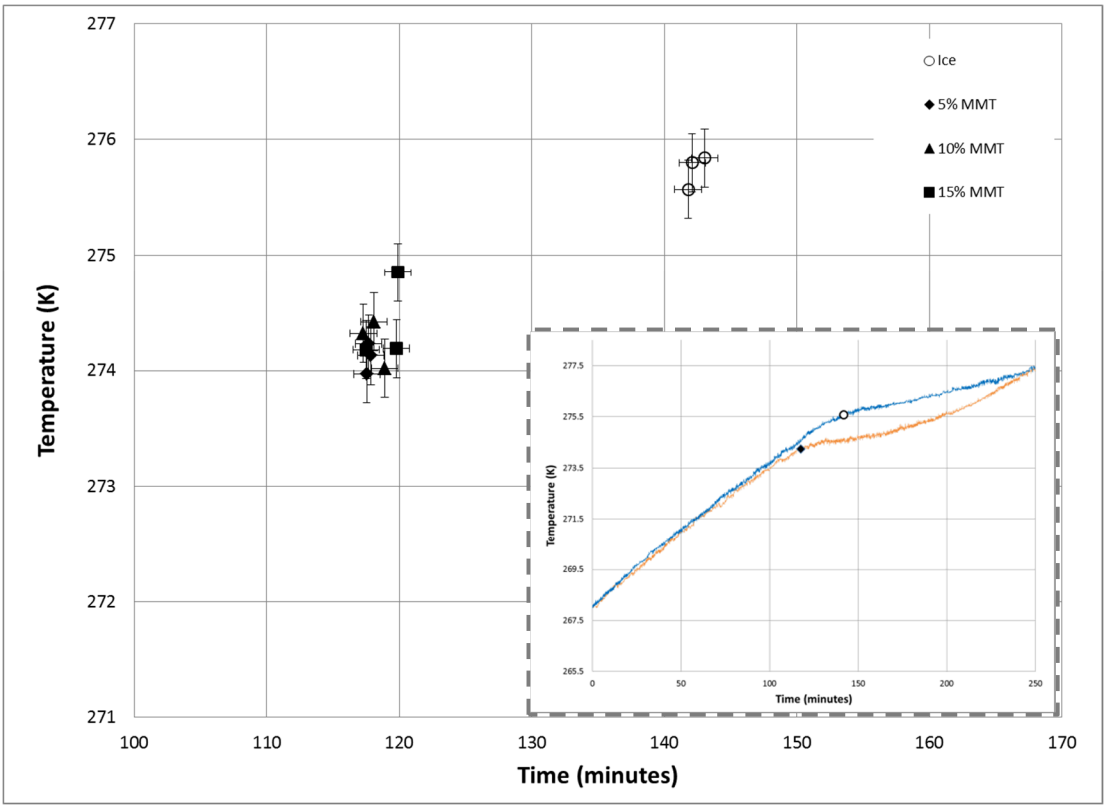

Figure 3: Temperature and time coordinates of the pressure deflection point for methane-ice and methane-ice-MMT clay samples. Filled black data points represent the deflection point of clay containing reactions, open data points represent pure ice and methane reactions. For clarity, one temperature data set each of the ice (blue line) and the 5% MMT reactions (orange line) is included in the lower right inset to show the course of the reaction progress over time. Refer to Figure 2 for full reaction profile.